JOURNAL OF SYNCHROTRON RADIATION
ISSN 1600-5775

Crystal structure of propionitrile (CH_3CH_2CN) determined using synchrotron powder X-ray diffraction

Helen E. A. Brand,[a]* Qinfen Gu,[a] Justin A. Kimpton,[a] Rebecca Auchettl[a] and Courtney Ennis[b,c]

[a]Australian Synchrotron, ANSTO, 800 Blackburn Road, Clayton, Victoria 3168, Australia, [b]University of Otago, PO Box 56, Dunedin 9054, New Zealand, and [c]Department of Chemistry and Physics, La Trobe Institute for Molecular Sciences, La Trobe University, Victoria 3086, Australia. *Correspondence e-mail: helenb@ansto.gov.au

Received 27 April 2019
Accepted 25 November 2019

Edited by A. F. Craievich, University of São Paulo, Brazil

Keywords: molecular ice; nitriles; planetary atmospheres; Titan.

Supporting information: this article has supporting information at journals.iucr.org/s

The structure and thermal expansion of the astronomical molecule propionitrile have been determined from 100 to 150 K using synchrotron powder X-ray diffraction. This temperature range correlates with the conditions of Titan's lower stratosphere, and near surface, where propionitrile is thought to accumulate and condense into pure and mixed-nitrile phases. Propionitrile was determined to crystallize in space group, *Pnma* (No. 62), with unit cell a = 7.56183 (16) Å, b = 6.59134 (14) Å, c = 7.23629 (14), volume = 360.675 (13) Å^3 at 100 K. The thermal expansion was found to be highly anisotropic with an eightfold increase in expansion between the c and b axes. These data will prove crucial in the computational modelling of propionitrile–ice systems in outer Solar System environments, allowing us to simulate and assign vibrational peaks in the infrared spectra for future use in planetary astronomy.

1. Introduction

Propionitrile (ethyl cyanide; CH_3CH_2CN) is an aliphatic nitrile commonly used as a solvent in chemical synthesis. Beyond Earth, gas-phase CH_3CH_2CN has been identified in a number of astrophysical environments. The strong dipole moment associated with the cyanide group (μ = 4.011 D: Kraśnicki & Kisiel, 2011) has led to the millimetre-wave detection of CH_3CH_2CN in the Orion nebula and molecular cloud Sagittarius B2 (Johnson *et al.*, 1977), as well as within the atmosphere of Saturn's moon Titan (Cordiner *et al.*, 2015). On Titan, CH_3CH_2CN is formed by neutral and ion chemistry between the photolytic products of molecular nitrogen and methane gas (Krasnopolsky, 2009; Dobrijevic *et al.*, 2016). Due to its low reactivity, CH_3CH_2CN is then thought to accumulate in the lower stratosphere before nucleation and growth of ices and aerosols (Coustenis *et al.*, 1999). However, the presence of pure CH_3CH_2CN ice has yet to be conclusively identified at these altitudes (Samuelson *et al.*, 2007) as opposed to other small nitriles that have been confirmed using infrared spectroscopy (Khanna, 2005). This leaves the required atmospheric sink for CH_3CH_2CN as an open question. It follows that mixed-phase cyanide ices incorporating CH_3CH_2CN have been proposed as the origin of Titan's mysterious 220 cm^{-1} feature (de Kok *et al.*, 2007; Jennings *et al.*, 2012). Concerning laboratory work on the condensed phase of CH_3CH_2CN, infrared studies have been performed in cryogenic matrices (Toumi *et al.*, 2015) and thin films (DelloRusso & Khanna, 1996; Moore *et al.*, 2010), as well as in the pure aerosol form

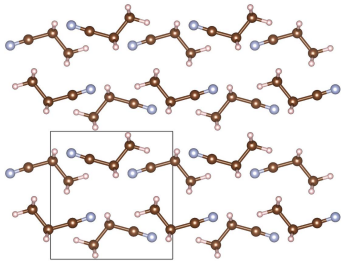

(Ennis *et al.*, 2017*a*). The latter investigation infers that a transition between two crystal phases may exist in the narrow temperature region between its ∼170 K melting point and 150 K. This mirrors the phase dependence of related acetonitrile (CH_3CN), which displays both low-temperature (α-phase: <160 K) and high-temperature (β-phase: 160–170 K) crystal structures (Antson *et al.*, 1987; Torrie & Powell, 1992; Enjalbert & Galy, 2002). Interestingly, it is often a metastable β-phase observed for low-temperature experiments involving the rapid condensation of CH_3CN ice (thin film and aerosol studies) due to the re-ordering of established dipole–dipole interactions being kinetically hindered (Tizek *et al.*, 2004).

Surprisingly for a common laboratory solvent, crystalline propionitrile has not yet been investigated by diffraction techniques. To bridge this gap in the fundamental solid-state structure of CH_3CH_2CN, this article reports on the results of a synchrotron powder X-ray diffraction study to (i) solve its low-temperature crystal structures and (ii) observe the thermal expansion behaviour of CH_3CH_2CN ice between 100 and 150 K. The determination of space group, lattice parameters and atomic coordinates has allowed our workgroup to undertake periodic density functional theory vibrational analysis (Civalleri *et al.*, 2007; Ennis *et al.*, 2017*b*) to assign and publish far-infrared spectra of CH_3CH_2CN ice obtained using a synchrotron source at temperatures consistent with Titan's atmosphere (Ennis *et al.*, 2018).

2. Sample preparation and data collection

The solvent sample (Sigma Aldrich, ≥99 GC Grade) was loaded into a 0.7 mm-diameter quartz glass capillary and mounted onto the powder diffraction beamline at the Australian Synchrotron (AS) (Wallwork *et al.*, 2007). The beamline was set up with a nominal wavelength of 1.0 Å; the wavelength was determined accurately using NIST SRM LaB_6 660b to be 0.99998 (1) Å. The sample was initially cooled to 100 K at 6 K min^{-1} using an Oxford Cryosystems Cryostream 700 and allowed to equilibrate for 10 min before the temperature was increased to 150 K where it was again allowed to equilibrate before a second cool to 100 K. Data were then collected upon warming in steps of 10 K from 100 to 150 K. Data were collected using the Mythen II microstrip detector (Schmitt *et al.*, 2003) from 3 to 83° in 2θ. To cover the gaps between detector modules, two data sets, each of 5 min in duration, were collected with the detector set 5° apart and these were then merged to give a single data set. Merging was performed using the in-house software *PDViPER*. A slit size of 2 mm was used, to ensure that the fraction of the capillary illuminated by the X-ray beam was the same as the isothermal zone on the cryostream. The capillary was rotated at ∼1 Hz during data collection to aid powder averaging. The cryostream equipment was calibrated at the beamline using a range of melting-point and phase-transition standards. Once these calibrations are applied, at the ramp rate used in this experiment, temperatures are accurate to within 1 K of the reported value.

3. Structure determination

The first 40° in 2θ of the 100 K dataset was indexed using *TOPAS5* software (Bruker AXS), to an orthorhombic unit cell. There is a broad impurity peak around 15.68°. The space group $Pna2_1$ (No. 33) was first assigned from analysis of the systematic absences. The reflection intensities were extracted using a Pawley fit with R_{wp} = 4.163%. The first attempt at structure solution, using the powder charge-flipping (CF) algorithm implemented in *Superflip* (Palatinus & Chapuis, 2007), was unsuccessful due to the high degree of preferred orientation (PO) of the sample. The crystal structure was then solved using a combination of the CF algorithm and the direct space method (with simulated annealing). After several trials with different preferred orientation settings, sixth-order spherical harmonic functions gave the best result. The CH_3CH_2CN molecule was defined as a rigid body unit in the simulated annealing procedure with idealized bond lengths (C—H = 1.0 Å, C—N = 1.16 Å, C—C = 1.53 Å) and bond angles from the ICDD organic database. Further symmetry analysis showed a higher possible symmetry in a non-isomorphic supergroup with the space group *Pnma* (No. 62). A subsequent Pawley fitting in *Pnma* gave R_{wp} = 4.197%, which is very similar to the fit given in the lower-symmetry space group $Pna2_1$.

Rietveld structural refinement was then conducted for this compound using this structural model in *Pnma* as shown in Fig. 1. All atomic bond lengths were set with restraints (less than 15% of the idealized bond values), while all bond angles were free to refine. The atomic displacement parameters of all atoms were constrained to be the same value. The Rietveld fit to the experimental powder X-ray diffraction data is excellent, yielding the agreement factors R_{wp} = 4.91%, R_B = 1.51%, goodness of fit (GoF) = 2.658. No additional atoms could be located by using difference Fourier maps. Table 1 provides details of the experimental setup and crystallographic results

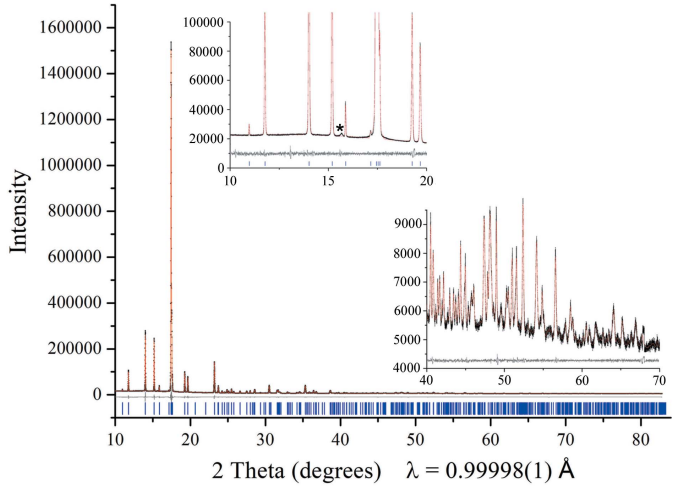

Figure 1
Rietveld fit of the proposed structural model (red) to observed diffraction data (black) at 100 K. The grey difference plot is shown below the data. Bragg peak positions are shown as blue bars. Note that there is a broad impurity peak around 15.68° marked by the asterisk (*).

Table 1
Experimental details.

Chemical formula	C_3H_5N
Formula weight	55.08 g mol^{-1}
Crystal system	Orthorhombic
Space group	*Pnma* (No. 62)
Cell parameters	a = 7.56183 (16) Å
	b = 6.59134 (14) Å
	c = 7.23629 (14) Å
Cell volume	360.675 (13) Å^3
Z	4
Calculated density	1.01427 g cm^{-3}
R_B	1.51%
R_{wp}	4.91%
GoF	2.658
2θ	$2\theta_{min}$ = 3°; $2\theta_{max}$ = 83°
Measured temperature	100 K
Diffractometer	Mythen-II, PD beamline
Radiation type	Synchrotron, AS
Wavelength	0.99998 (1) Å

Table 2
Fractional atomic coordinates for propionitrile at 100 K.

Wyck = Wyckoff position. SOF = standard occupancy factor.

Atom	Wyck	SOF	x/a	y/b	z/c	B
N1	4c	1	0.1711 (2)	1/4	0.8291 (2)	2.02 (4)
C1	4c	1	0.1110 (3)	1/4	0.3522 (3)	2.02 (4)
C2	4c	1	0.2684 (3)	1/4	0.4826 (3)	2.02 (4)
C3	4c	1	0.2172 (2)	1/4	0.6802 (3)	2.02 (4)
H1	8d	1	0.0305 (12)	0.3779 (15)	0.3661 (15)	2.02 (4)
H2	8d	1	0.3419 (13)	0.1230 (11)	0.4658 (14)	2.02 (4)
H3	4c	1	0.149 (2)	1/4	0.212 (2)	2.02 (4)

obtained. Due to the weak scattering of H atoms from X-rays, we next conducted first-principles calculations to determine the optimized crystal structure. Density functional theory (DFT) calculations were conducted with the *VASP* 5.4.4 code (Kresse & Hafner, 1993) on Australian Synchrotron Computer Infrastructure (ACSI). The generalized gradient approximation (Kresse & Hafner, 1993) with a Perdew–Burke–Ernzerhof (Perdew *et al.*, 1996) exchange correlation function was used. The atomic potentials of C $2s^2\ 2p^2$, N $2s^2\ 2p^3$ and H $1s^1$ were treated by ultra-soft pseudo potentials (Kresse & Joubert, 1999). The zero damping DFT-D3 dispersion correction method of Grimme was used to account for the significance of van der Waals interactions in the system (Larijani *et al.*, 2017). The cut-off energy of 800 eV and Monkhorst Pack k-point of 5 × 5 × 5 were used to converge the total energy of the system within 1 meV atom^{-1}. In the structural relaxation calculation, all atoms were allowed to relax within a fixed unit cell.

4. Crystal structure description

Fig. 2 shows the structure of CH_3CH_2CN viewed along each crystallographic axis in 2 × 2 × 2 unit cells. Propionitrile was determined to crystallize in space group *Pnma* (No. 62), with unit cell a = 7.56183 (16) Å, b = 6.59134 (14) Å, c = 7.23629 (14), volume = 360.675 (13) Å^3 at 100 K. Fractional atomic coordinates can be found in Table 2. Crystallographic density is calculated to be 1.01427 g cm^{-3}. The CH_3CH_2CN molecules are arranged in chains along the c-axis which form layers in the ac plane. The CH_3CH_2CN molecules are reversed in their orientation in neighbouring chains along the a-axis. The planes are stacked along the b-axis with an interplane distance of 3.295 (1) Å.

The arrangement of CH_3CH_2CN molecules within the crystalline structure is almost identical to the gas-phase monomer r_s-structure (Table 3), as determined by analysis of the microwave spectra recorded from selected CH_3CH_2CN isotopologues (Heise *et al.*, 1974). In the latter r_s-structure, the molecule deviates slightly from C_s symmetry, with disparate bond-lengths for the internal CH_3 group resulting in a rotated minimum and the CCN angle measured less than the expected

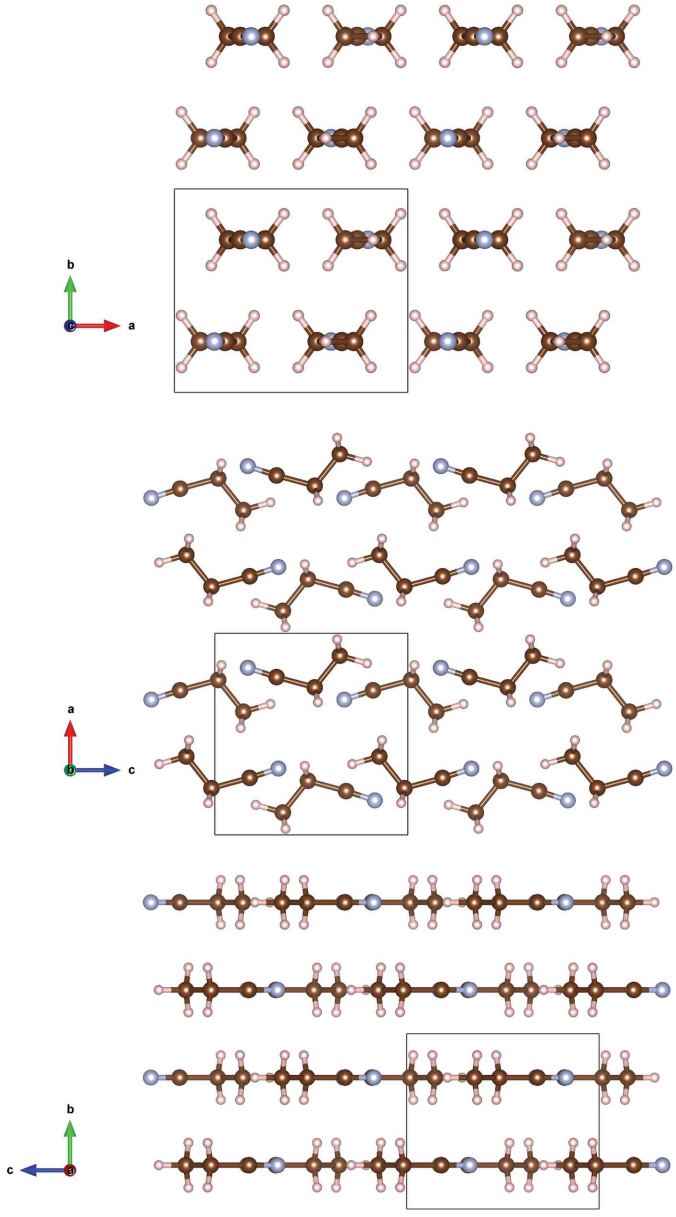

Figure 2
Packing of CH_3CH_2CN presented in 2 × 2 × 2 unit-cells. Nitrogen is blue, carbon brown and hydrogen pink.

Table 3
Structural parameters of CH_3CH_2CN at 100 K compared with experimental gas-phase values.

Bond lengths				Bond angles				
Atom 1	Atom 2	Bond length (Å)	Gas-phase molecule†	Atom 1	Central atom	Atom 3	Angle (°)	Gas-phase molecule†
N1	C3	1.1325 (3)	1.159 (1)	N1	C3	C2	177.2 (2)	178.73
C1	C2	1.5189 (3)	1.537 (1)	C3	C2	C1	113.3 (2)	111.98
C2	C3	1.481 (3)	1.459 (1)					
				C3	C2	H2	105.0 (6)	108.13
C2	H2	1.01 (8)	1.094 (1)	C1	C2	H2	110.8 (5)	110.62
				C2	C1	H1	113.4 (5)	111.08
C1	H1	1.045 (9)	1.079 (18)	C2	C1	H3	112.6 (8)	110.47
C1	H3	1.05 (1)	1.091 (1)					
				Dihedral angle (H3C1–C2H2)			62.243 (9)	59.31

† Heise, Lutz & Dreizler (1974), r_s-structure.

Table 4
Thermal expansion parameters of solid CH_3CH_2CN.

	a-axis	*b*-axis	*c*-axis
a (K^{-2})	–	6.598×10^{-6}	8.308×10^{-7}
b (K^{-1})	1.094×10^{-3}	1.260×10^{-4}	1.148×10^{-4}
L_0 (Å)	7.453	6.514	7.217
R^2 (%)	99.98	99.94	99.86

180°. The two internal C—C bond lengths suggest a degree of double-bond character over the aliphatic backbone of the molecule (Lerner & Dailey, 1957). This is mirrored in the molecular structure upon crystallization with relatively minor deviation from the gas-phase structure. The maximum deviation is 4% reduction in the C—H bond lengths on the methyl group. This is unsuprising as X-ray measurements are least sensitive to hydrogen positions.

All bond angles are observed to be similarly identical from crystalline to gas-phase, particularly those associated with the C—H aliphatic hydrogens where deviation is of the order of 2–3° while the aliphatic carbon backbone only displays a slight opening of less than 2°. The dihedral angle as measured from the carbon backbone is 62.2 (9)°, again only a 3° deviation.

Between the molecules within the structure, the H2 hydrogen of the CH_3 moiety is coordinated toward the lone electron pair of the nitrile N1 atom associated with the neighbouring molecule at an interatomic distance of 2.65 (8) Å. There appears to be no close packing of neighbouring nitrile groups indicating that dipole–dipole interactions are secondary to interactions between intermolecular C–H and nitrile moieties.

5. Thermal expansion of propionitrile

The volume thermal expansion of CH_3CH_2CN between 100 and 150 K can be described simply using a polynomial of the form: $V = aT^2 + bT + V_0$, where $a = 4.237\,(1) \times 10^{-4}$, $b = 6.051\,(1) \times 10^{-2}$ and $V_0 = 350.53\,(1)$, with an agreement of $R^2 = 99.95\%$. The lack of data points means that it is not reasonable to further manipulate the data to, for example, extract the expansivity tensor. Fig. 3 shows the volume expansion of the unit cell. The unit-cell axes have also been fitted with polynomials, the *a*- and *c*-axes with a second-order polynomial and the *b*-axis with a linear fit. These coefficients are shown in Table 4.

Fig. 4 shows the relative axial expansivities of the unit-cell axes. The *b*-axis has the highest expansivity: at 150 K it is double that of the *a*-axis and eight times the *c*-axis. This is not unexpected as monomers are held together by hydrogen bonding only parallel to the *b*-axis – see Fig. 2.

In order to easily compare the expansivity of CH_3CH_2CN with ice, the polynomial fit to the data has been differentiated and used in equation (1),

$$a_v = \frac{1}{V_0}\left(\frac{\partial V}{\partial T}\right). \quad (1)$$

Fig. 5 shows the experimental expansivity determined here for CH_3CH_2CN compared with that of ice 1_h over the same temperature range. The expansivity of CH_3CH_2CN is similar to ice 1_h in magnitude and linearity, which follows from the

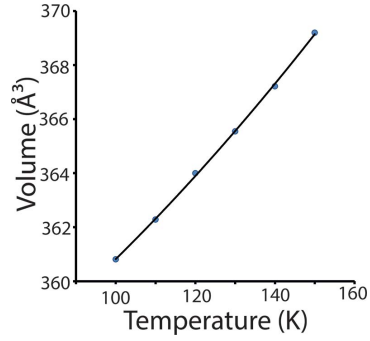

Figure 3
Thermal expansion of unit-cell volume for solid CH_3CH_2CN between 100 and 150 K. Errors are approximately the same size as the data points.

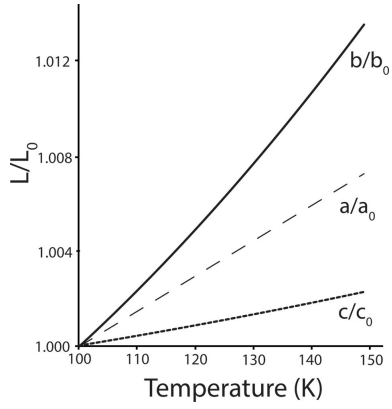

Figure 4
Relative expansivities of the unit-cell axes between 100 and 150 K. The *a*-axis is represented by a dotted line, the *b*-axis by a dashed line and the *c*-axis by a full line. The '0' subscript denotes that the expansions are relative to the lowest temperature value.

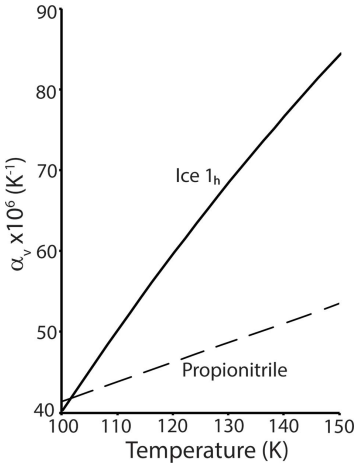

Figure 5
Relative volume expansivity of propionitrile compared with ice 1_h after Röttger *et al.* (1994).

simplicity and few data points of the form of the volume expansion data for CH_3CH_2CN.

6. Summary and future directions

Synchrotron X-ray powder diffraction has been used to determine the crystal structure and thermal expansion of CH_3CH_2CN from 100 to 150 K under ambient pressure conditions. The CH_3CH_2CN molecules are arranged in chains along the *c*-axis.

The volume thermal expansion is positive and similar in magnitude to that of ice 1_h under the same conditions. However, the expansivity of ice 1_h increases at a higher rate than that of CH_3CH_2CN suggesting the two may have complex interactions in environments where they are found together. The expansivity of CH_3CH_2CN is more in line with that of materials such as highly hydrated sulfates found in the Jovian system.

The small variation between the gas-phase molecular structure and that observed here is likely a result of a differing measurement temperature: 200 K in the literature and 100 K here. The changes in specific bond lengths and angles may give a hint to the important structural constructs which control the thermal expansion.

However, they are merely hints and further X-ray powder diffraction measurements are warranted, perhaps combined with neutron diffraction measurements, over a more granular temperature range to obtain details of the behaviour of the hydrogen-bonding network and elastic strain tensor. This and a full investigation of the phase relations of the CH_3CH_2CN–H_2O system will be crucial if we are to understand the behaviour of CH_3CH_2CN over the range of temperatures found from the surface of Titan through the atmosphere to the Orion nebula.

Funding information

This work was carried out on the powder diffraction beamline at the Australian synchrotron; supported by Australian Research Council via the Discover Early Career Research Award (DE150100301). RA was supported by an Australian Government Research Training Program (RTP) Scholarship. RA also thanks the Australian Institute of Nuclear Science and Engineering (AINSE) for their financial support under the AINSE Postgraduate Research Award (PGRA) scheme to enable this work

References

Antson, O. K., Tilli, K. J. & Andersen, N. H. (1987). *Acta Cryst.* B**43**, 296–301.
Civalleri, B., Doll, K. & Zicovich-Wilson, C. M. (2007). *J. Phys. Chem. B*, **111**, 26–33.
Cordiner, M. A., Palmer, M. Y., Nixon, C. A., Irwin, P. G. J., Teanby, N. A., Charnley, S. B., Mumma, M. J., Kisiel, Z., Serigano, J., Kuan, Y. J., Chuang, Y. L. & Wang, K. S. (2015). *Astrophys. J.* **800**, L14.
Coustenis, A., Schmitt, B., Khanna, R. K. & Trotta, F. (1999). *Planet. Space Sci.* **47**, 1305–1329.
de Kok, R., Irwin, P. G. J., Teanby, N. A., Nixon, C. A., Jennings, D. E., Fletcher, L., Howett, C., Calcutt, S. B., Bowles, N. E., Flasar, F. M. & Taylor, F. W. (2007). *Icarus*, **191**, 223–235.
Dobrijevic, M., Loison, J. C., Hickson, K. M. & Gronoff, G. (2016). *Icarus*, **268**, 313–339.
Enjalbert, R. & Galy, J. (2002). *Acta Cryst.* B**58**, 1005–1010.
Ennis, C., Auchettl, R., Appadoo, D. R. T. & Robertson, E. G. (2017*b*). *Mon. Not. R. Astron. Soc.* **471**, 4265–4274.
Ennis, C., Auchettl, R., Appadoo, D. R. T. & Robertson, E. G. (2018). *Phys. Chem. Chem. Phys.* **20**, 23593–23605.
Ennis, C., Auchettl, R., Ruzi, M. & Robertson, E. G. (2017*a*). *Phys. Chem. Chem. Phys.* **19**, 2915–2925.
Heise, H. M., Lutz, H. & Dreizler, H. (1974). *Z. Naturforsch. A*, **29**, 1345.
Jennings, D. E., Anderson, C. M., Samuelson, R. E., Flasar, F. M., Nixon, C. A., Kunde, V. G., Achterberg, R. K., Cottini, V., de Kok, R., Coustenis, A., Vinatier, S. & Calcutt, S. B. (2012). *Astrophys. J.* **754**, L3.
Johnson, D. R., Lovas, F. J., Gottlieb, C. A., Gottlieb, E. W., Litvak, M. M., Thaddeus, P. & Guelin, M. (1977). *Astrophys. J.* **218**, 370–376.
Khanna, R. K. (2005). *Icarus*, **178**, 165–170.
Kraśnicki, A. & Kisiel, Z. (2011). *J. Mol. Spectrosc.* **270**, 83–87.
Krasnopolsky, V. A. (2009). *Icarus*, **201**, 226–256.
Kresse, G. & Hafner, J. (1993). *Phys. Rev. B*, **47**, 558–561.
Kresse, G. & Joubert, D. (1999). *Phys. Rev. B*, **59**, 1758.
Larijani, H. T., Jahanshahi, M., Ganji, M. D. & Kiani, M. H. (2017). *Phys. Chem. Chem. Phys.* **19**, 1896–1908.
Lerner, R. G. & Dailey, B. P. (1957). *J. Chem. Phys.* **26**, 678–680.
Moore, M. H., Ferrante, R. F., James Moore, W. & Hudson, R. (2010). *Astrophys. J. Suppl.* **191**, 96–112.
Palatinus, L. & Chapuis, G. (2007). *J. Appl. Cryst.* **40**, 786–790.
Perdew, J. P., Burke, K. & Ernzerhof, M. (1996). *Phys. Rev. Lett.* **77**, 3865–3868.
Röttger, K., Endriss, A., Ihringer, J., Doyle, S. & Kuhs, W. F. (1994). *Acta Cryst.* B**50**, 644–648.
Russo, N. D. & Khanna, R. K. (1996). *Icarus*, **123**, 366–395.
Samuelson, R. E., Smith, M. D., Achterberg, R. K. & Pearl, J. C. (2007). *Icarus*, **189**, 63–71.
Schmitt, B., Brönnimann, C., Eikenberry, E. F., Gozzo, F., Hörmann, C., Horisberger, R. & Patterson, B. (2003). *Nucl. Instrum. Methods Phys. Res. A*, **501**, 267–272.
Tizek, H., Grothe, H. & Knözinger, E. (2004). *Chem. Phys. Lett.* **383**, 129–133.
Torrie, B. H. & Powell, B. M. (1992). *Mol. Phys.* **75**, 613–622.
Toumi, A., Piétri, N. & Couturier-Tamburelli, I. (2015). *Phys. Chem. Chem. Phys.* **17**, 30352–30363.
Wallwork, K. S., Kennedy, B. J. & Wang, D. (2007). *AIP Conf. Proc.* **879**, 879–882.